Finite Element Modeling and Experimental Characterization of Crosstalk in 1-D CMUT Arrays

Baris Bayram, *Student Member, IEEE*, Mario Kupnik, Goksen G. Yaralioglu, *Member, IEEE*, Ömer Oralkan, *Member, IEEE*, Arif Sanli Ergun, *Member, IEEE*, Der-Song Lin, Serena H. Wong, *Student Member, IEEE*, and Butrus T. Khuri-Yakub, *Fellow, IEEE*

***Abstract*—Crosstalk is the coupling of energy between the elements of an ultrasonic transducer array. This coupling degrades the performance of transducers in applications such as medical imaging and therapeutics. In this paper, we present an experimental demonstration of guided interface waves in capacitive micromachined ultrasonic transducers (CMUTs). We compare the experimental results to finite element calculations using a commercial package (LS-DYNA) for a 1-D CMUT array operating in the conventional and collapsed modes. An element in the middle of the array was excited with a unipolar voltage pulse, and the displacements were measured using a laser interferometer along the center line of the array elements immersed in soybean oil. We repeated the measurements for an identical CMUT array covered with a 4.5-μm polydimethylsiloxane (PDMS) layer. The main crosstalk mechanism is the dispersive guided modes propagating in the fluid-solid interface. Although the transmitter element had a center frequency of 5.8 MHz with a 130% fractional bandwidth in the conventional operation, the dispersive guided mode was observed with the maximum amplitude at a frequency of 2.1 MHz, and had a cut-off frequency of 4 MHz. In the collapsed operation, the dispersive guided mode was observed with the maximum amplitude at a frequency of 4.0 MHz, and had a cut-off frequency of 10 MHz. Crosstalk level was lower in the collapsed operation (−39 dB) than in the conventional operation (−24.4 dB). The coverage of the PDMS did not significantly affect the crosstalk level, but reduced the phase velocity for both operation modes. Lamb wave modes, A_0 and S_0, were also observed with crosstalk levels of −40 dB and −65 dB, respectively. We observed excellent agreement between the finite element and the experimental results.**

I. Introduction

Ultrasound transducers in immersion are subject to the crosstalk between the neighboring array elements. This crosstalk degrades the transducer performance for applications such as diagnostic imaging and high intensity focused ultrasound (HIFU) treatment in medicine. In general, crosstalk increases the effective element aperture and the ringdown time of a transducer, resulting in a poor angular response and range resolution [1]. In imaging experiments using capacitive micromachined ultrasonic transducers (CMUTs), degradation in the axial resolution and bright patterns in the near field were observed due to crosstalk [2]. HIFU applications require the precise control of the focal point for power deposition to the pathological regions without destroying the surrounding healthy tissues [3]. However, because of a wider beamwidth and higher sidelobes, the crosstalk impairs the transducer's capability to focus the ultrasound tightly [4].

Experimental, analytical, and finite element methods are used to determine the causes and effects of crosstalk in CMUTs. Common experimental methods are optical displacement and electrical received signal measurements. Other methods such as pulse-echo and radiation pattern measurements are also employed to analyze crosstalk [5]. The spatial resolution of the electrical measurements, unlike optical measurements, is limited by the width of the array element. Due to finer spatial resolution in the optical measurements, the laser interferometry is generally preferred to investigate the crosstalk. The coupling on CMUT arrays was investigated in immersion using laser interferometry [6]; however, the displacement measurements were not corrected for the acousto-optic interactions between the laser beam and the pressure field in the fluid. Because of the acousto-optic interactions, the uncorrected optical measurements result in the overamplification of the displacement measurements associated with the waves propagating at the speed of sound in the fluid [7]. A method to account for this effect was presented in [7].

The presence of highly dispersive waves causing crosstalk in CMUTs was analytically shown in [8]. The supported modes were also calculated numerically as a function of the phase relation between neighboring cells in [9], [10]. Two-dimensional (2-D) CMUT models were simulated by taking the periodicity of the structure and the radiation conditions into account [9], and this analysis was extended to 3-D CMUT models [10]. This efficient computational model combines the finite element and the boundary element methods to perform the harmonic analysis of a periodic CMUT structure.

Using a more computation-intensive approach compared to the harmonic analysis, time-domain finite element analysis (FEA) of a 2-D CMUT model was performed

Manuscript received April 10, 2006; accepted August 22, 2006. This work was supported by the United States Office of Naval Research under grant N00014-02-1-0007, and National Institutes of Health under grants CA99059 and HL67647. M. Kupnik acknowledges the FWF Austrian Science Fund for financial support.

All authors except B. Bayram are currently with the Edward L. Ginzton Laboratory, Stanford University, Stanford, CA 94305 (e-mail: bbayram@gmail.com).

All authors were with the Edward L. Ginzton Laboratory when this reasearch was performed.

Digital Object Identifier 10.1109/TUFFC.2007.256

using ANSYS (ANSYS Inc., Canonsburg, PA), and the crosstalk level between the neighboring elements was determined to be −22 dB in immersion [11]. A 3-D, time-domain finite element model (FEM) was developed for CMUT arrays using PZFlex (Weidlinger Associates Inc., Los Altos, CA) [12]. The explicit solver used in PZFlex enables the modeling of larger structures. An interface wave, propagating at a velocity of 1000 m/s, was observed in the 1-D CMUT array simulation [12].

Previously, we investigated the dynamic behavior of CMUTs in the conventional and collapsed modes of operation by using a time-domain, finite element package (LS-DYNA, Livermore Software Technology Corporation, Livermore, CA) [13]. LS-DYNA, based on an explicit solver, features robust contact capability and electrostatic-structural coupling via user-defined subroutines [14]. We verified the FEM results with the interferometer measurements in [13].

In this paper, we analyze the crosstalk performance of a 1-D CMUT array by comparing the finite element calculations and the experimental measurements in both conventional and collapsed modes. The FEM is constructed by taking advantage of the symmetries of the 1-D CMUT array. As in the experiment, the model of the array is 41 elements long, but infinite in the elevation direction. The FEM also represents the exact surface topology and material composition of the actual array, which was fabricated using the conventional sacrificial release process. We observed excellent agreement between the FEM and the experimental results. The crosstalk wave consists of three distinct components: S_0 Lamb wave mode (−65 dB normalized to the maximum transmitter displacement), A_0 Lamb wave mode (−40 dB), and the dispersive guided mode (−24.4 dB). The crosstalk level of the dispersive guided mode is lower in the collapsed operation (−39 dB) than in the conventional operation (−24.4 dB). The polydimethylsiloxane (PDMS) coverage is relatively ineffective in reducing crosstalk.

The organization of this paper is as follows: Section II briefly describes the 1-D CMUT array used in this study. The FEM and the LS-DYNA calculations are explained in Section III. The details of the experimental work using laser interferometer are given in Section IV. The results are presented in Section V, and discussed in Section VI.

Compared to the existing FEA in literature, our FEA is distinguished by having all five main features together: First, the explicit, time domain solver of LS-DYNA enables the modeling of the actual CMUT array in detail, i.e., all 41 array elements are modeled. Second, user-defined subroutines provide an efficient electrostatic-structural coupling method. Third, the robust contact capability offers the CMUT modeling in collapsed operation. Fourth, a fast method to bias the CMUT array in the conventional and collapsed modes is implemented. Fifth, the FEA results are verified with interferometer measurements. The main focus of this paper is to explain the main crosstalk mechanism in CMUT arrays and to verify our finite element calculations by experimental results.

TABLE I
PHYSICAL PARAMETERS OF THE 1-D CMUT ARRAY.

Number of elements	41
Size of an element, μm × μm	250 × 6000
Number of cells in element width	5
Center-to-center cell spacing, μm	40
Membrane radius (r_m), μm	18
Membrane wall thickness (t_{w1}), μm	0.6
Oxide wall thickness (t_{w2}), μm	0.4
Electrode radius (r_e), μm	9
Membrane thickness (t_m), μm	0.63
Electrode thickness (t_e), μm	0.30
Passivation layer thickness (t_p), μm	0.45
Gap thickness (t_g), μm	0.095
Insulation layer thickness (t_i), μm	0.205
Silicon substrate thickness (t_s), μm	500

II. 1-D CMUT ARRAY

A 41-element central section of a 64-element 1-D CMUT array was used in the experiments [Fig. 1(a)]. The center element was the transmitter, and 20 elements on each side were used for receive. Each array element was 6 mm long and 250 μm wide [Fig. 1(b)]. The array elements were composed of circular cells [Fig. 1(c)]. Each array element included five cells along the width, and the center-to-center cell separation was 40 μm [Fig. 1(d)]. The inner and outer radii of the etch holes were 2 μm and 4 μm, respectively [Fig. 1(d)]. The physical dimensions of the CMUT array are given in Table I.

To investigate the effects of a surface coating on crosstalk, an identical CMUT array was covered with PDMS (model 1-4105 conformal coating elastomer; Dow Corning Co., Midland, MI). PDMS is a biocompatible material and provides electrical isolation to the active areas of each element for use of CMUTs in contact with living tissue. This particular material was preferred because of its low viscosity. A 4.5-μm-thick layer was uniformly formed by spin coating at 3000 rpm. The bond wires were covered by the UV-cured epoxy (Norland Optical Adhesive 61; Thorlabs Inc., Newton, NJ) to protect them from detachment due to the centrifugal force during the spin coating.

We measured the center frequency of CMUT in air to be 10 MHz at 5-V DC bias. CMUT cells initially started collapsing at 30 V, and all the cells were collapsed at 32 V. A white light 3-D surface profiler (New View 100; Zygo Corporation, Middlefield, CT) was used to measure the peak static deflection of 0.024 μm under the atmospheric pressure of 1 atm. The gap of 0.095 μm was also verified by measuring the difference between the zero-bias and collapse-state center deflections.

III. FINITE ELEMENT CALCULATIONS

We modeled the 1-D CMUT array for the finite element calculations as shown in Fig. 2(a). Because of the symmetry of the actual 41-element array around the center of

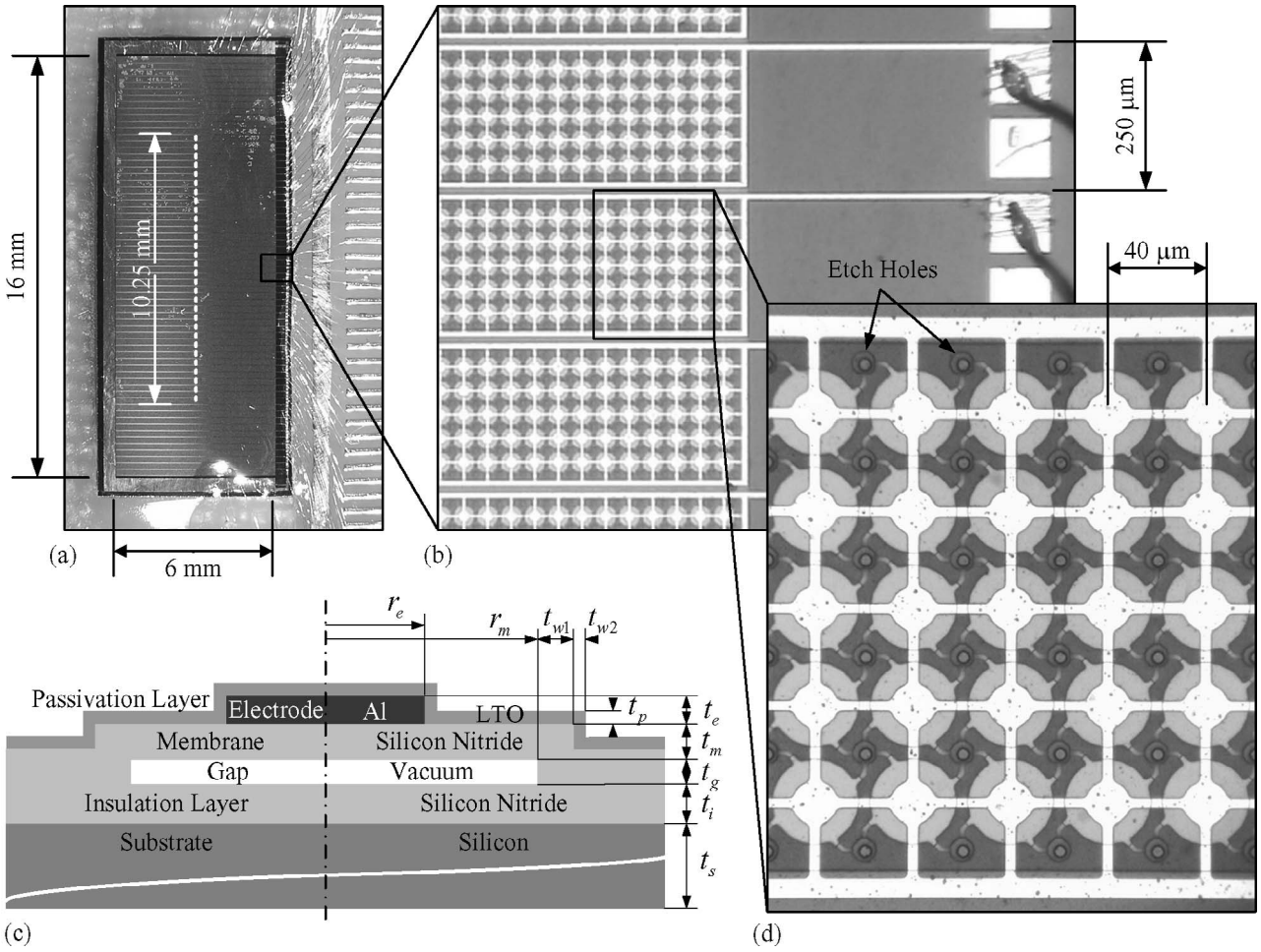

Fig. 1. 1-D CMUT array: (a) top view of the complete 1-D CMUT array on the PCB; (b) three elements of the 1-D CMUT array; (c) schematic cross section of a CMUT cell; (d) magnified view of a single 5-cell-wide, 1-D CMUT array element.

the transmitter, only half of the array was included in the model. The symmetry along the length of each element allowed modeling half of the circular membranes [Fig. 2(b)]. The substrate and epoxy thicknesses were 500 μm and 200 μm, respectively. The soybean oil height was 3000 μm. The close-ups of an array element and a cell are shown in Fig. 2(c) and (d), respectively. The dimensions of the cell in the FEM are the same as the physical dimensions described in Table I and Fig. 1(c).

ANSYS/LS-DYNA, a commercially available FEM package, was used to define the solid geometry, to mesh the structure, and to generate the final input deck for the LS-DYNA calculations. We described FEA of CMUTs using LS-DYNA in our previous publications [13], [15], [16]. Finite element models for the half-element [includes only the transmitter in Fig. 2(b)] and the 20-element [includes the transmitter and 20 receiver elements in Fig. 2(b)] are compared in Table II. The deformed nodal positions under the bias voltage and the atmospheric pressure (1 atm) were calculated for the half-element model using the dynamic relaxation function of LS-DYNA [14]. Then, ANSYS/LS-DYNA and MATLAB (The MathWorks Inc., MA) were used to expand the deformed nodal results of the half-element model to the matching nodal results of the 20-element model. This approach made the biasing of CMUT array faster because the number of elements in the calculation was reduced to 2.5% of the 20-element model (Table II). Following the biasing of the CMUT array, we performed the dynamic analysis of the 20-element model.

TABLE II
FINITE ELEMENT MODEL INFORMATION.

Finite element model	Half-element	20-element
Number of elements	45160	1851560
Number of nodes	43567	1729087
Number of lines	5313	212033
Number of areas	4598	186198
Number of volumes	1316	53956

The ground electrode was beneath the insulation layer. The top electrode was made of aluminum sandwiched between the silicon nitride membrane and the oxide layer. The ideal contact elements (no friction, no binding forces) were defined on the top and bottom surfaces of the vacuum gap.

We defined electrostatic-structural coupled forces within the electrodes using the user-defined loading fea-

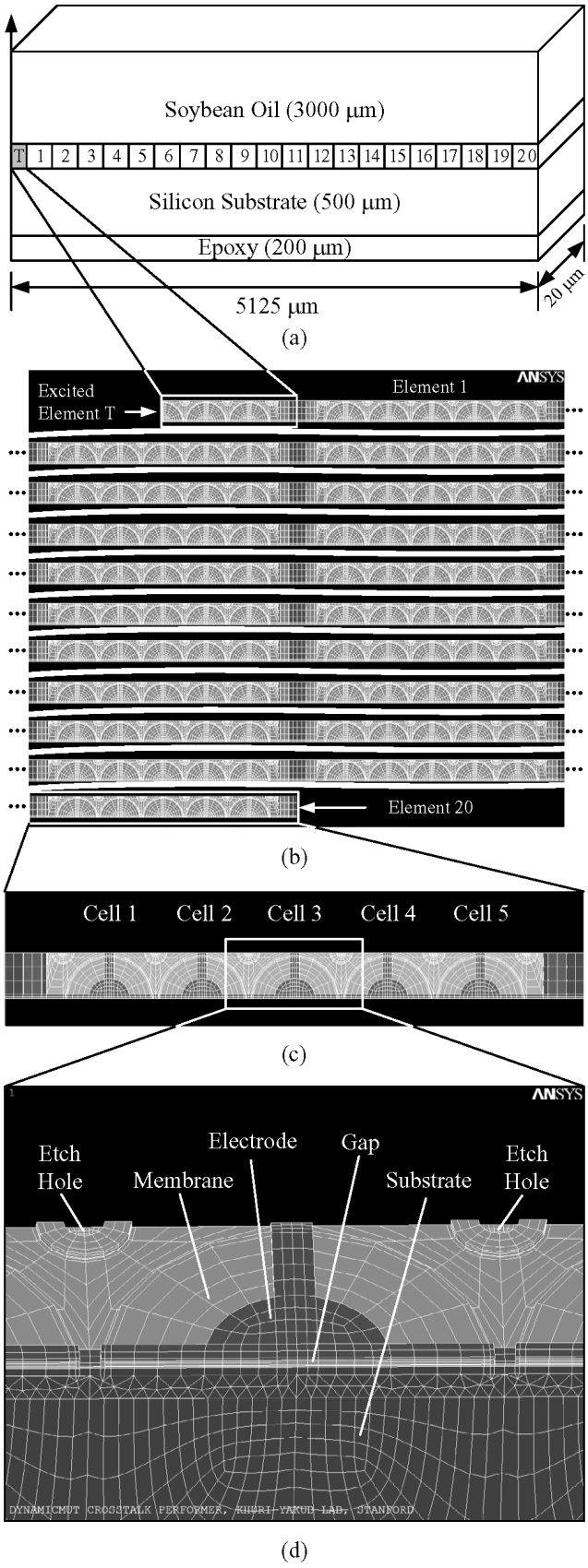

Fig. 2. Finite element model (FEM) of the 1-D CMUT array: (a) schematic description of the complete FEM; (b) top view of CMUT surface; (c) magnified view of one CMUT array element surface; (d) magnified, perspective view of one CMUT cell.

ture of LS-DYNA [13], [14]. These forces were also verified for both conventional and collapsed modes of operation using the coupled-field approach described in [15]. Because the post-processing of the large model required significant disk space and computer time, we used the user-defined material feature of LS-DYNA to write the displacement and the pressure over the whole array surface directly to a text file [14]. These data were collected with a time step of 10 ns for a total time of 4 μs. The simulation was performed using LS-DYNA executable (ver. 970-5434d) on a workstation (dual-processor 3 GHz Dell Precision 470; Dell Inc., Round Rock, TX) with a Linux operating system (GNU).

The material properties used in the LS-DYNA calculations are given in Table III. The relative dielectric permittivities of the Si_3N_4 and the vacuum were used to calculate the electrostatic forces acting on the electrodes due to the applied voltage. Both soybean oil and PDMS were modeled with fluid-like characteristics, and the attenuation of the PDMS was taken into consideration. The epoxy under the silicon substrate had a lower impedance than the silicon substrate. No displacement boundary conditions were specified in the epoxy or the substrate.

We calculated the center frequency of CMUT in air to be 10 MHz at 5-V DC bias, as observed experimentally. However, the collapse voltage of CMUT was calculated to be 85 V in FEA, whereas it was measured to be 32 V in the experiments. Using the membrane deflection profiles of CMUT measured using the white light interferometer, we matched the corresponding experimental and FEA voltages by matching the deflection profiles. Bias voltages of 25 V (conventional mode) and 40 V (collapsed mode) in the experiments were equivalent to 75 V (conventional mode) and 100 V (collapsed mode) in the FEA, respectively. The collapse voltage difference between the FEM calculations and the experiments was possibly due to the charging in the CMUT membrane and insulation layer [17], which is currently under investigation. The ratio of gap height (0.095 μm) to the silicon nitride thickness (0.63 μm) is small enough to cause a large collapse voltage variation in our CMUT array as a result of this charging. Although this charging phenomenon shifts the collapse voltage of the CMUT, it does not significantly affect the crosstalk characteristics.

IV. Experimental Work

The experimental setup was designed to perform optical and electrical measurements simultaneously, as described in [18] (Fig. 3). The optical measurement system was explained in [13].

The CMUT array was immersed in soybean oil, and the laser beam was focused on the array surface. Using a computer-controlled translational stage, the laser beam was scanned along the reflective metal line in the middle of the array [Fig. 1(a)]. To account for the acousto-optic interactions, the pressure integral along the laser path in oil needs to be known as a function of time [7]. Experimen-

TABLE III
MATERIAL PROPERTIES USED IN FINITE ELEMENT ANALYSIS.

	Si	Si_3N_4	LTO	Al	Epoxy	PDMS	Soybean oil	Vacuum
Young's modulus (GPa)	169	320	60	67.6	3			
Density (kg/m^3)	2332	3270	2200	2700	1100	1020	930	
Poisson's ratio	0.290	0.263	0.170	0.355	0.400			
Velocity of sound (m/s)						1080	1485	
Relative permittivity		5.7						1
Attenuation (dB/cm)						6.5		

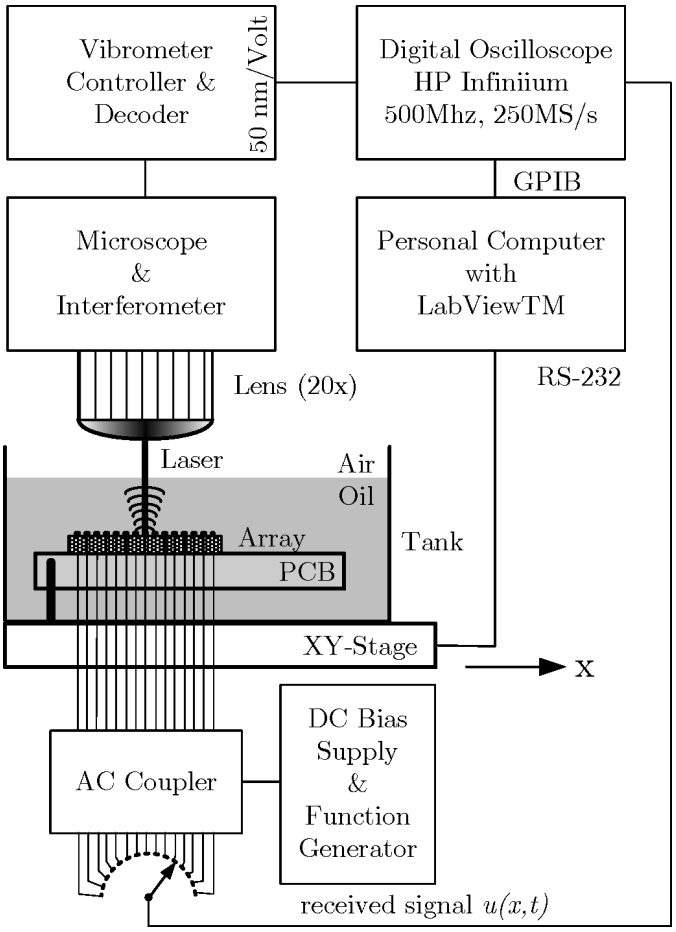

Fig. 3. Experimental setup used in the optical and electrical measurements.

tally, the acousto-optic correction can be implemented easily based on the following two assumptions: 1) The optical data gathered on the posts can be attributed directly to the pressure integral along the laser path in oil because the displacement of the posts between the membranes is negligible compared to the membrane displacement; 2) The pressure integrals on the CMUT cell and its posts are approximately equal to each other because the distance between the CMUT membrane and its posts (20 μm) is only a fraction of the wavelength (300 μm at 5 MHz). Following the correction for the pressure field in oil, the actual membrane displacements are obtained by using the refractive index of soybean oil ($n_{\text{oil}} = 1.47$) in the optical path calculation.

The optical displacement waveform, corrected for the acousto-optic effect, showed good agreement with the electrical received signal in [18], confirming the validity of optical measurements. Because the spatial resolution of the electrical measurements was limited by the array width of 250 μm, we present only the optical measurements with the spatial resolution of 5 μm, determined by the laser spot diameter (Fig. 3).

The CMUT array was biased in the conventional and collapsed modes of operation. A 20-ns, +10-V unipolar pulse was applied to the transmitter element. The pulse amplitude and duration were selected such that the transmitter element did not accidentally operate in the collapse-snapback mode described in [19]. The interferometer output signal was collected with a time step of 4 ns for a total time of 4 μs.

V. RESULTS

A. Conventional Mode of Operation

In the FEM displacement results presented in the time-spatial domain [Fig. 4(a)], three components of crosstalk propagating with different phase velocities and signal strengths are observed. The fastest crosstalk component is the weakest, with −65 dB displacement amplitude relative to the transmitter. A slightly slower component is observed at −40 dB level, and the slowest component is the strongest, at −24.4 dB. One should also note that the pressure data presented in Fig. 4(b) do not show any discontinuities, as observed in the corresponding displacement data [Fig. 4(b)].

Although the time-spatial domain representation provides insight about the nature of crosstalk, the identification of different wave types is difficult in this approach. Therefore, a transformation into the frequency-wavenumber domain is required to analyze propagating multi-mode signals [20].

The FEM and experimental displacement results are compared in the frequency-wavenumber domain, as depicted in Fig. 4(c) and (d), respectively. A dispersive guided mode is observed with the maximum amplitude at a frequency of 2.1 MHz, and has a cut-off frequency of

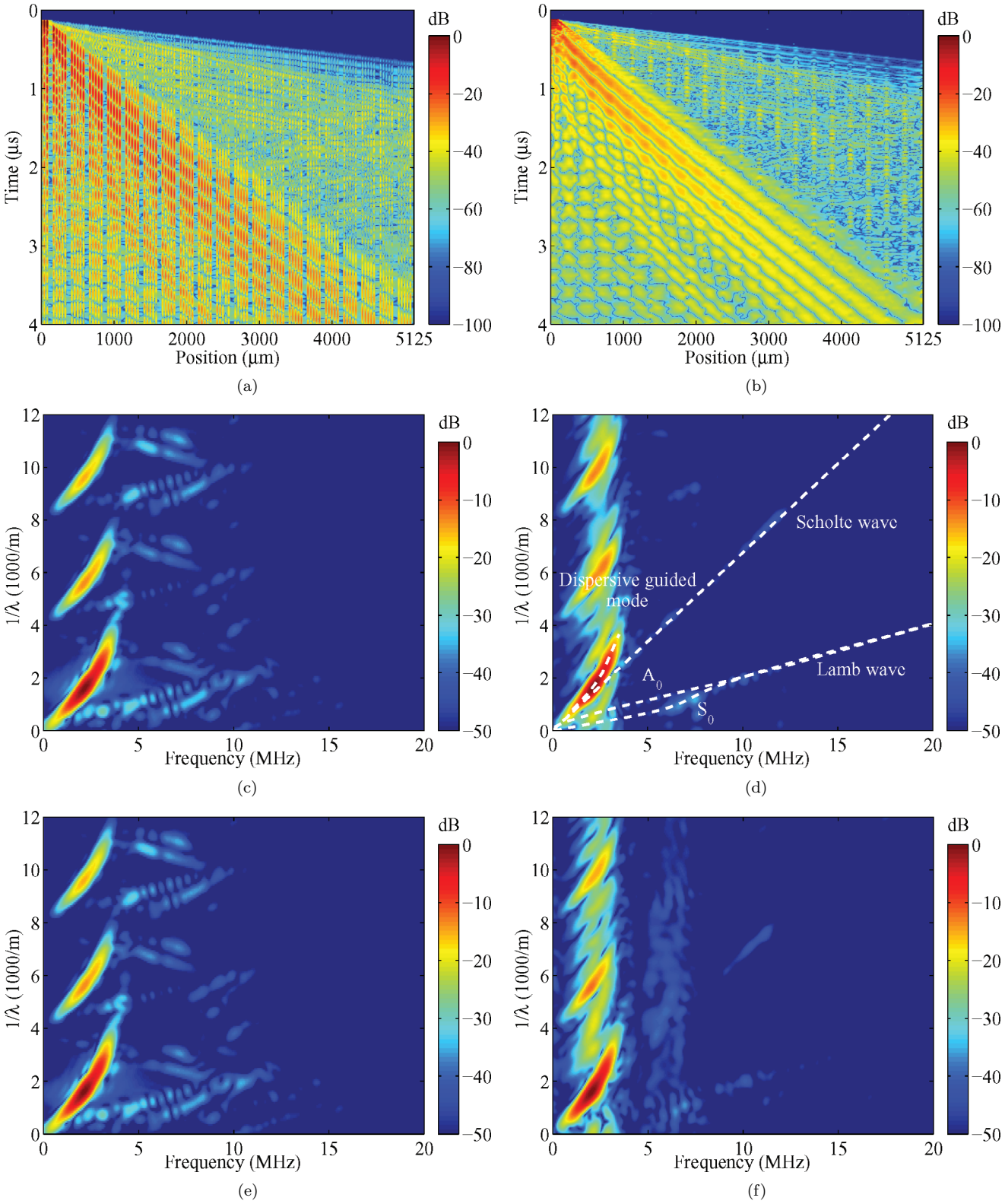

Fig. 4. Crosstalk waves of 1-D CMUT array in the conventional mode of operation: (a) FEM displacement results in the time-spatial domain; (b) FEM pressure results in the time-spatial domain; (c) FEM displacement results in the frequency-wavenumber domain; (d) experimental displacement results in the frequency-wavenumber domain; (e) FEM displacement results for the PDMS-covered CMUT array in the frequency-wavenumber domain; (f) experimental displacement results for the PDMS-covered CMUT array in the frequency-wavenumber domain.

4 MHz. The multiples of the guided mode are separated by 4 mm^{-1}, which corresponds to the array pitch of 250 μm. These multiples do not represent any physical wave. Although a weak wave in the vicinity of the dispersive guided mode at a velocity of 620 m/s is observed in the experiments, it does not appear in the FEM results. Therefore, this experimental result is an artifact. In both FEM and experimental results, Lamb wave modes (A_0 and S_0) are also observed, and are coincident with the theoretically calculated curves for a 500-μm substrate [Fig. 4(d)] [21]. The FEM and experimental displacement results for the 1-D CMUT array, covered with PDMS, are compared in Fig. 4(e) and (f), respectively. The PDMS coverage does not significantly affect the results presented in Fig. 4(c) and (d) for the CMUT array without PDMS.

B. Collapsed Mode of Operation

The FEM calculations and the experimental measurements were repeated for the collapsed mode of operation. Compared to that in the conventional mode, the crosstalk amplitude of the dispersive guided mode (both displacement and pressure) was smaller in the collapsed mode [Fig. 5(a) and (b)].

The FEM and experimental displacement results are compared in the frequency-wavenumber domain in Fig. 5(c) and (d), respectively. The dispersive guided mode has the maximum amplitude at a frequency of 4.0 MHz, and has a cut-off frequency of 10 MHz. Because the crosstalk level associated with the dispersive guided mode is approximately 14.6 dB less in the collapsed operation, Lamb wave modes (A_0 and S_0) appear to be stronger in this case [Fig. 5(c)]. The FEM and experimental displacement results for the 1-D CMUT array, covered with the PDMS, are also presented for comparison in Fig. 5(e) and (f). Although the PDMS coverage reduces the crosstalk level by 4.3 dB in the experiments, no change is observed in the FEM results.

C. Crosstalk Comparison

To analyze the displacement frequency response of the transmitter and its neighbor (Element 1), the displacement was averaged over these elements. In the conventional mode, the resulting FEM and experimental frequency spectra show good agreement, as shown in Fig. 6(a) and (b). The crosstalk displacement on Element 1 had a normalized peak value of approximately −10 dB at 2.1 MHz and a dip at 4.0 MHz. The corresponding pressure frequency response for the excited element had a center frequency of 5.8 MHz with a 130% fractional bandwidth in the conventional operation. In the collapsed mode, the crosstalk displacement on Element 1 had a peak value of approximately −22 dB at multiple frequencies around 3.5 MHz and 8.5 MHz [Fig. 6(a)]. A dip at 5.8 MHz was observed between these peaks. This dip is not observed in experiments because of limited accuracy in optical methods. The corresponding pressure frequency response for the excited element had a center frequency of 12.4 MHz with a 90% fractional bandwidth.

Using the average displacement data, we calculated the relative crosstalk level for all elements in the array. The crosstalk amplitude on Element 1 was −17 dB in the conventional mode without the PDMS coverage for both FEM and experimental results, as shown in Fig. 7(a) and (b), respectively. This amplitude decreased almost linearly with the distance from the transmitter element. The crosstalk amplitude on Element 18 was −32 dB and −30 dB for the FEM and the experiment, respectively. The crosstalk level averaged over the neighboring elements in Fig. 7(a) was −24.4 dB and −23.2 dB for the FEM and experiment, respectively. The PDMS coverage did not significantly affect the crosstalk level. Compared to the conventional mode, the collapsed mode had the crosstalk level of −28 dB on Element 1 and −39 dB on average for all of the neighboring elements in Fig. 7(a). This FEM result corresponded to 14.6 dB better crosstalk level in collapsed mode. The crosstalk level of −21 dB on Element 1 and −34.4 dB on average for the neighboring elements was obtained for the experiment [Fig. 7(b)]. The average crosstalk level with the PDMS coverage was −39 dB and −38.7 dB for the FEM and the experiment, respectively [Fig. 7(b)].

We extracted the dispersion relation of the guided interface mode from the frequency-wavenumber representations. At lower frequencies, the phase velocity approached the velocity of sound in the fluid (1485 m/s) [Fig. 8(a) and (b)] in all cases. The phase velocity monotonically decreased with increasing frequencies up to the cut-off frequency, above which the propagation of this mode is not supported. The cut-off frequency for the collapsed operation (10 MHz) was higher than the cut-off frequency for the conventional operation (4 MHz). The coverage of the PDMS reduced the phase velocity for the conventional and the collapsed operations in both FEM and experimental results.

VI. Discussion

The crosstalk in the 1-D CMUT array was investigated using laser interferometry and LS-DYNA simulations. Although both the displacement and pressure were available from the FEM calculations, only displacement measurements were possible using an interferometer. To compare the FEM and the experimental results side by side, we chose to use the displacement results for frequency-wavenumber domain representations. The multiples of the dispersive guided mode, corresponding to 250-μm separation, were observed in the spectra. The periodic array elements were composed of the vibrating membrane surfaces (5 circular cells, each 40 μm in diameter) and the substrate surfaces (50 μm) between the neighboring elements. The presence of the almost stationary substrate surface between the array elements resulted in the generation of the multiples. Because of the linear interpolation scheme between the data points, the presence of the multiples for

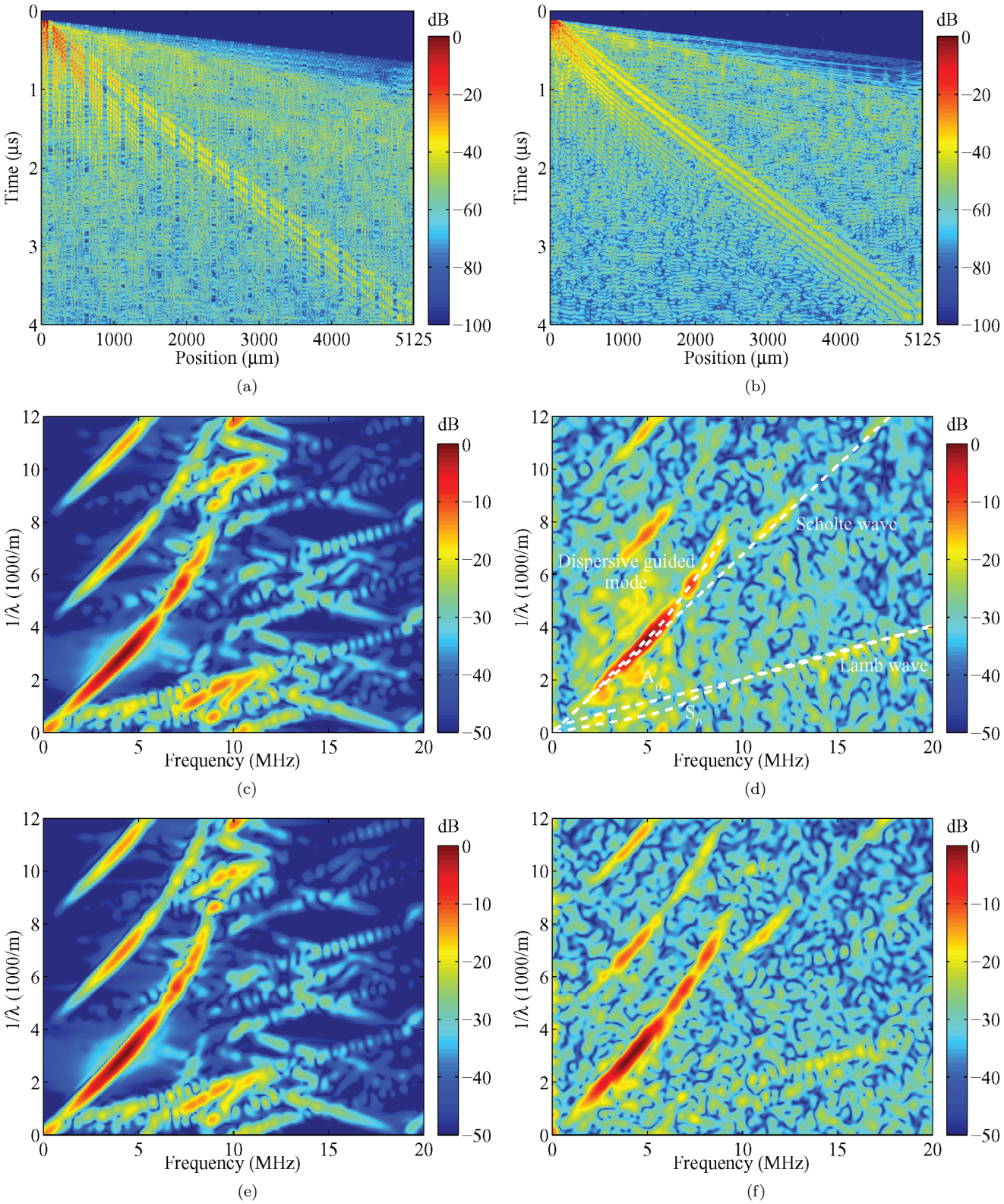

Fig. 5. Crosstalk waves of 1-D CMUT array in the collapsed mode of operation: (a) FEM displacement results in the time-spatial domain; (b) FEM pressure results in the time-spatial domain; (c) FEM displacement results in the frequency-wavenumber domain; (d) experimental displacement results in the frequency-wavenumber domain; (e) FEM displacement results for the PDMS-covered CMUT array in the frequency-wavenumber domain; (f) experimental displacement results for the PDMS-covered CMUT array in the frequency-wavenumber domain.

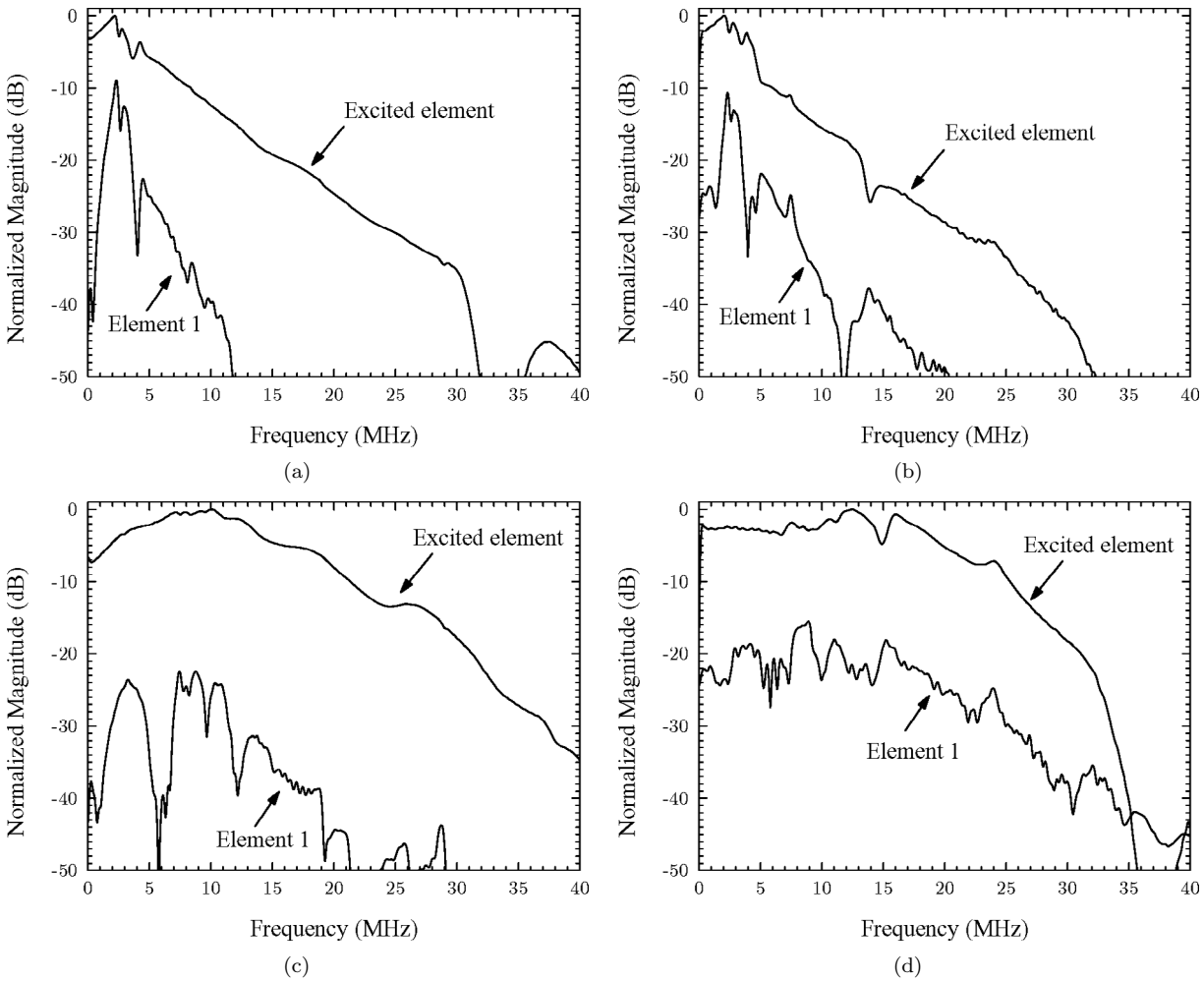

Fig. 6. Spectra of excited element and element 1: (a) FEM spectra in the conventional mode of operation; (b) experimental spectra in the conventional mode of operation; (c) FEM spectra in the collapsed mode of operation; (d) experimental spectra in the collapsed mode of operation.

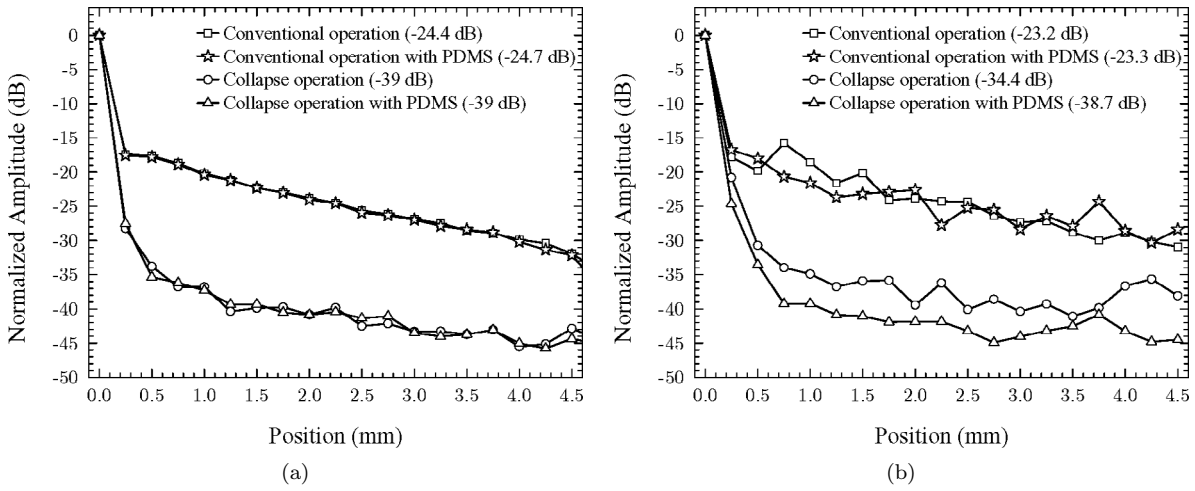

Fig. 7. Crosstalk-normalized amplitudes of array elements in the conventional and collapsed modes of operation: (a) FEM results; (b) experimental results.

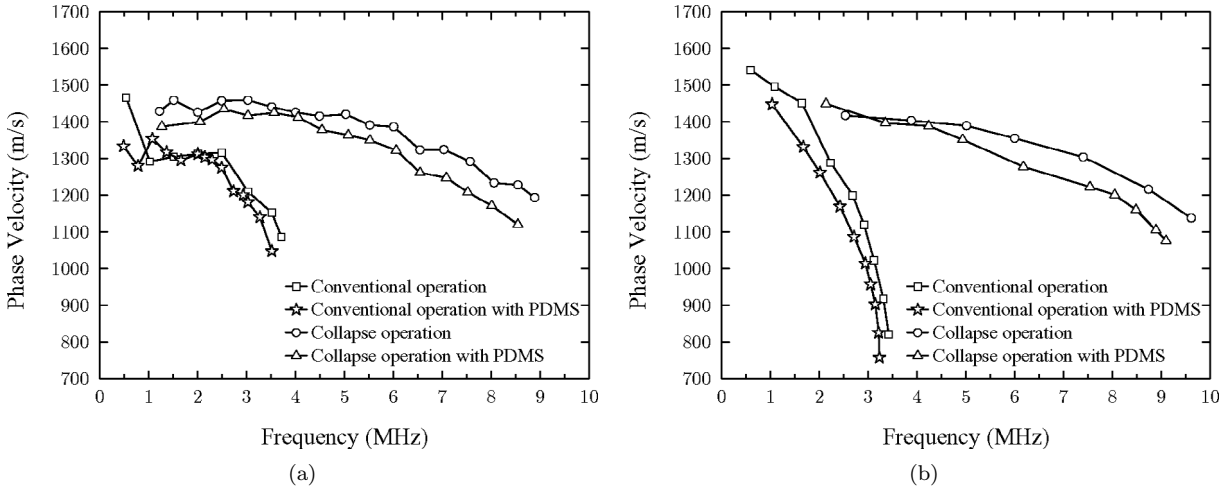

Fig. 8. Phase velocity of dispersive guided mode in the conventional and collapsed modes of operation: (a) FEM results; (b) experimental results.

5-μm spatial resolution in the experiment was not observed for the data with 40-μm spatial resolution in [18].

The Lamb wave modes (A_0 and S_0) in the frequency-wavenumber domain have higher signal strength in the FEM than in the experimental results. This discrepancy is related to the acousto-optic correction implemented for the experimental results. In our acousto-optic correction, we assume that the optical measurements on the posts (the separation region) of the membranes are entirely due to the pressure field in the oil. In reality, the Lamb wave modes also contribute to the actual displacements of the posts. Because of the presence of Lamb waves, the correction reduces their relative signal strength in the frequency-wavenumber domain. Another acousto-optic correction method, described in [7], does not cause the problem of reduction in the Lamb waves. However, this method completely removes all of the waves propagating at the phase velocity of the sound in the oil (1485 m/s), and generates a strong artificial wave propagating at approximately 1880 m/s for soybean oil. Our correction method describes the guided modes without introducing these artifacts at a cost of reduced Lamb waves.

Although the PDMS coverage does not make significant change in the calculated and measured crosstalk levels in conventional operation, the crosstalk level in the collapsed operation is reduced from -34.4 dB to -38.7 dB in experiments, and is -39 dB in calculations [Fig. 7(a) and (b)]. In the model, the frequency-independent attenuation of 6.5 dB/cm was used for PDMS. However, the attenuation of PDMS is a function of frequency, and proportional to $f^{1.4}$ [22]. In the collapsed operation, the frequency of operation is approximately doubled, and causes higher attenuation. In future work, frequency-dependent attenuation will be used for PDMS.

The excited element had a center frequency of 5.8 MHz with a 130% fractional bandwidth in the conventional operation. However, the neighboring element (Element 1) was narrow band in nature, and had a center frequency of 2.1 MHz. The discrepancy between the center frequency of transmission and reception was due to the different phase relation in each case. During transmission, five cells of the excited element were all pulsed in phase. In-phase excitation caused higher center frequency and higher fractional bandwidth for the element than the frequency and bandwidth of each individual cell. The cells of the neighboring element picked up the crosstalk waves sequentially along the interface during reception. Therefore, the phase delay between the cells in reception resulted in a lower center frequency (2.1 MHz) during reception, compared to a higher center frequency (5.8 MHz) during in-phase transmission. An important advantage of the collapsed mode over the conventional mode was the lower crosstalk level. Increase of the cut-off frequency from 4 MHz in the conventional mode to 10 MHz in the collapsed mode was a result of the higher membrane resonance in collapse. The center frequencies are also higher in the collapsed operation, and result in higher phase delay between the cells and lower crosstalk levels.

In the conventional mode, the 3-dB bandwidth in transmission extends from 2 MHz to 9.6 MHz. The guided mode has the peak at 2.1 MHz, and this frequency can be lowered by reducing the phase delay between the neighboring cells [10]. The guided mode disappears close to 4 MHz, corresponding to the membrane resonance in immersion. Therefore, a frequency band (4–9.6 MHz) is available for transmission without the effects of guided interface modes. In this case, the crosstalk level will be approximately -40 dB due to the A_0 lamb wave mode, which corresponds to more than a 15-dB improvement. A frequency band (10–18 MHz) without the presence of the guided modes is also observed in the collapsed mode.

The stiffness and density of the membrane affect the phase velocity of the guided mode [8]. The arrangement of the membranes within the array element influences the preferred frequency of the guided mode as a result of the phase delay between the adjacent cells [10]. Due to the frequency dependence of the guided modes, a CMUT array that has crosstalk outside the bandwidth of the transducer

can be designed for exceptional crosstalk performance using flexible parameters, e.g., the dimensions of the membrane, the gap, and the insulation layer.

VII. Conclusion

We investigated the crosstalk in the 1-D CMUT array by laser interferometry and LS-DYNA calculations. Both the theoretical calculations and the experimental measurements agreed that the dispersive guided modes, supported by the membrane resonance, played the most important role in the crosstalk between the neighboring elements. The crosstalk amplitude on the first neighboring element was −17 dB, in good agreement with [6] and [11]. Compared to the conventional operation (−24.4 dB), the collapsed operation of CMUT resulted in a 14.6-dB better crosstalk level (−39 dB). The cut-off frequency for the collapsed operation (10 MHz) was higher than the cut-off frequency for the conventional operation (4 MHz). Due to the dispersion, the phase velocity of the guided mode, approaching the speed of sound in the fluid (1485 m/s) at lower frequencies, decreased monotonically with increasing frequency and disappeared above the cut-off frequency for both conventional and collapsed operations. The coverage of the PDMS reduced the phase velocity for the conventional and the collapsed operations, but did not significantly affect the crosstalk amplitude.

LS-DYNA can be used to accurately model the crosstalk in CMUT arrays under specific voltage bias and excitation conditions. Such a modeling is well worth the effort for special-purpose CMUT arrays for ultrasound applications such as medical imaging and HIFU treatment. Our verified LS-DYNA model will be used to investigate the methods of crosstalk reduction in future work.

Acknowledgment

The authors would like to thank Dr. Wayne L. Mindle from Livermore Software Technology Corporation (LSTC) for providing technical assistance in LS-DYNA and providing the object files for user-defined loading implementation, Dr. Khanh Bui from LSTC for providing useful information about the coupled-field analysis using LS-DYNA, Dr. Morten Rikard Jensen from LSTC for providing technical support for full restart and dynamic relaxation implementations in LS-DYNA, Dr. Fabio Mantovani for compiling the LS-DYNA executable for our GNU linux operating system, and Dr. Scott Rodamaker from MCR Associates, Inc., for providing technical support in ANSYS and ANSYS/LS-DYNA.

References

[1] J. F. Dias, "An experimental investigation of the cross coupling between elements of an acoustic imaging array transducer," *Ultrason. Imag.*, vol. 4, pp. 1137–1139, 1982.

[2] Ö. Oralkan, A. S. Ergun, J. A. Johnson, M. Karaman, U. Demirci, K. Kaviani, T. H. Lee, and B. T. Khuri-Yakub, "Capacitive micromachined ultrasonic transducers: Next-generation arrays for acoustic imaging?," *IEEE Trans. Ultrason., Ferroelect., Freq. Contr.*, vol. 49, pp. 1596–1610, Nov. 2002.

[3] C. Zanelli, "Design and characterization of a 10 cm annular array transducer for high intensity focused ultrasound (HIFU) applications," in *Proc. IEEE Ultrason. Symp.*, 1994, pp. 144–148.

[4] S. Zhou, G. L. Wojcik, and J. A. Hossack, "An approach for reducing adjacent element crosstalk in ultrasound arrays," *IEEE Trans. Ultrason., Ferroelect., Freq. Contr.*, vol. 50, pp. 1752–1761, Dec. 2003.

[5] X. C. Jin, Ö. Oralkan, F. L. Degertekin, and B. T. Khuri-Yakub, "Characterization of one-dimensional capacitive micromachined ultrasonic immersion transducer arrays," *IEEE Trans. Ultrason., Ferroelect., Freq. Contr.*, vol. 48, pp. 750–759, May 2001.

[6] A. Caronti, D. Fiasca, G. Caliano, M. Pappalardo, and E. Cianci, "Experimental study of acoustic coupling in CMUT arrays by optical interferometry," in *Proc. IEEE Ultrason. Symp.*, 2003, pp. 909–914.

[7] D. Certon, G. Ferin, O. B. Matar, J. Guyonvarch, J. P. Remenieras, and F. Patat, "Influence of acousto-optic interactions on the diffracted field by an array obtained from displacement measurements," *Ultrasonics*, vol. 42, pp. 465–471, 2004.

[8] P.-C. Eccardt, A. Lohfink, and H.-G. von Garssen, "Analysis of crosstalk between fluid coupled cmut membranes," in *Proc. IEEE Ultrason. Symp.*, 2005, pp. 593–596.

[9] S. Ballandras, M. Wilm, W. Daniau, A. Reinhardt, V. Laude, and R. Armani, "Periodic finite element/boundary element modeling of capacitive micromachined ultrasonic transducers," *J. Appl. Phys.*, vol. 97, no. 3, pp. 034901–034907, 2005.

[10] M. Wilm, A. Reinhardt, V. Laude, and S. Ballandras, "Three-dimensional modeling of micromachined-ultrasonic-transducer arrays operating in water," in *Ultrasonics*, vol. 43, no. 6, pp. 457–465, May 2005.

[11] Y. Roh and B. T. Khuri-Yakub, "Finite element analysis of underwater capacitor micromachined ultrasonic transducers," *IEEE Trans. Ultrason., Ferroelect., Freq. Contr.*, vol. UFFC-49, pp. 293–298, Mar. 2002.

[12] G. Wojcik, J. Mould, P. Reynolds, A. Fitzgerald, P. Wagner, and I. Ladabaum, "Time-domain models of MUT array cross-talk in silicon substrates," in *Proc. IEEE Ultrason. Symp.*, 2000, pp. 909–914.

[13] B. Bayram, G. G. Yaralioglu, M. Kupnik, A. S. Ergun, Ö. Oralkan, A. Nikoozadeh, and B. T. Khuri-Yakub, "Dynamic analysis of capacitive micromachined ultrasonic transducers," *IEEE Trans. Ultrason., Ferroelect., Freq. Contr.*, vol. 52, no. 12, pp. 2270–2275, Dec. 2005.

[14] LS-DYNA 970 Keyword User's Manual, Livermore Software Technology Corporation, Livermore, CA, 2003.

[15] B. Bayram, E. Hæggström, G. G. Yaralioglu, and B. T. Khuri-Yakub, "A new regime for operating capacitive micromachined ultrasonic transducers," *IEEE Trans. Ultrason., Ferroelect., Freq. Contr.*, vol. 50, pp. 1184–1190, Sep. 2003.

[16] B. Bayram, G. G. Yaralioglu, A. S. Ergun, Ö. Oralkan, and B. T. Khuri-Yakub, "Dynamic FEM analysis of multiple cMUT cells in immersion," in *Proc. IEEE Ultrason. Symp.*, 2004, pp. 252–255.

[17] X. Yuan, J. C. M. Hwang, D. Forehand, and C. L. Goldsmith, "Modeling and characterization of dielectric-charging effects in RF MEMS capacitive switches," *IEEE MTT-S Int. Microw. Symp. Dig.*, pp. 753–756, 2005.

[18] B. Bayram, M. Kupnik, G. G. Yaralioglu, Ö. Oralkan, D. Lin, X. Zhuang, A. S. Ergun, A. F. Sarioglu, S. H. Wong, and B. T. Khuri-Yakub, "Characterization of cross-coupling in capacitive micromachined ultrasonic transducers," in *Proc. IEEE Ultrason. Symp.*, 2005, pp. 601–604.

[19] B. Bayram, Ö. Oralkan, A. S. Ergun, E. Hæggström, G. G. Yaralioglu, and B. T. Khuri-Yakub, "Capacitive micromachined ultrasonic transducer design for high power transmission," *IEEE Trans. Ultrason., Ferroelect., Freq. Contr.*, vol. 52, no. 2, pp. 326–339, Feb. 2005.

[20] D. Alleyne and P. Cawley, "A two-dimensional fourier transformation method for the measurement of propagating multimode signals," *J. Acoust. Soc. Amer.*, vol. 89, pp. 1159–1168, 1991.

[21] F. L. Degertekin and B. T. Khuri-Yakub, "Lamb wave excitation by hertzian contacts with applications in NDE," *IEEE Trans. Ultrason., Ferroelect., Freq. Contr.*, vol. 44, pp. 769–779, Jul. 1997.

[22] J. D. Fraser, "The design of efficient, broadband ultrasonic transducers," Ph.D. dissertation, Stanford University, Stanford, CA, 1979.

Baris Bayram (S'02) was born in Izmir, Turkey, in 1977. He received the B.S. degree in 2000 from Bilkent University, Ankara, Turkey; and the M.S. and Ph.D. degrees in 2002 and 2006, respectively, from Stanford University, Stanford, CA, all in electrical engineering. From 2000 to 2006, he was a Research Assistant at Khuri-Yakub Ultrasonics Group, E. L. Ginzton Laboratory, Stanford University.

His research interests include design, fabrication, and characterization of capacitive micromachined ultrasonic transducers (CMUTs). He particularly investigates the nonlinear operation regimes (collapsed and collapse-snapback) of CMUTs for high acoustic output performance, and novel CMUT designs for better crosstalk performance using static and dynamic packages such as ANSYS and LS-DYNA for the accurate finite element modeling of CMUTs.

He has 3 pending patents related to operation modes and crosstalk of CMUTs, and co-authored 8 journal and 13 conference publications. He is a student member of the IEEE.

Mario Kupnik was born in Leoben, Austria, in 1974. He received his M.S. degree in electronics engineering from the Graz University of Technology, Graz, Austria, in 2000. From summer 1999 to October 2000, he worked as an Analog Design Engineer for Infineon Technologies AG, Graz, on the design of ferroelectric memories and contactless smart card systems. From 2000 to 2004, he worked as a research assistant at the Christian Doppler Laboratory for Sensory Measurement, c/o Institute for Automation, University of Leoben, Leoben, Austria. He received his Ph.D. in physical measurement techniques from the University of Leoben in 2004 for his research in ultrasonic flow metering of hot gaseous mixtures, focusing especially on the exhaust gases of automotive combustion engines.

He is currently a postdoctoral researcher in the Khuri-Yakub Ultrasonics Group at the E. L. Ginzton Laboratory at Stanford University, Stanford, CA. His research interests include the design and application of capacitive micromachined ultrasonic transducers, focusing especially on ultrasonic transit-time gas flowmeters for hot and pulsating gases, and on ultrasonic nondestructive evaluation. Dr. Kupnik received the 2004 Fred-Margulies Award of the International Federation of Automatic Control (IFAC). He holds four patents in the fields of analog front-end circuits for contactless smart card systems and ultrasonic transit-time gas flowmeters.

Goksen Goksenin Yaralioglu (S'92–M'99) was born in Akhisar, Turkey on May 13, 1970. He received his B.S., M.S., and Ph.D. degrees from Bilkent University, Ankara, Turkey, in 1992, 1994, and 1999, respectively, all in electrical engineering. He is now working as an engineering research associate in E. L. Ginzton Laboratory, Stanford University, Stanford, CA. His current research interests include design, modeling and applications of micromachined ultrasonic transducers, and atomic force microscopy at ultrasonic frequencies.

Ömer Oralkan (S'93–M'05) received the B.S. degree from Bilkent University, Ankara, Turkey, in 1995, the M.S. degree from Clemson University, Clemson, SC, in 1997, and the Ph.D. degree from Stanford University, Stanford, CA, in 2004, all in electrical engineering.

Currently, he is an engineering research associate at the E. L. Ginzton Laboratory at Stanford University. His past and present research interests include analog and digital circuit design, micromachined sensors and actuators, and semiconductor device physics and fabrication. His current research focuses on the design and implementation of integrated ultrasonic imaging systems.

Dr. Oralkan received the 2002 Outstanding Paper Award of the IEEE Ultrasonics, Ferroelectrics, and Frequency Control Society. He is a member of the IEEE.

Arif Sanli Ergun (S'91–M'99) was born in Ankara, Turkey in 1969. He received his B.Sc., M.Sc., and Ph.D. degrees in 1991, 1994 and 1999, respectively, all in electrical and electronics engineering from Bilkent University, Ankara, Turkey. He is now in E. L. Ginzton Laboratory, Stanford University, Stanford, CA, as an engineering research associate. His main research interests are acoustics, ultrasound, microelectromechanical systems (MEMS), and microwave electronics.

Der-Song Lin received the B.S. and M.S. degrees in civil engineering from National Taiwan University, Taipei, Taiwan, in 1995 and 1997 with the master research of Non-Destructive-Evaluation, and the M.S. degree in mechanical engineering from Stanford University, Stanford, CA, in 2006. He is currently working toward the Ph.D. degree in mechanical engineering at Stanford University.

He worked as a consultant engineer in Sinotech Engineering Consultant Inc., Taipei, Taiwan, from 1999 to 2001. He joined Redin International, Inc., Taipei, Taiwan, as a special assistant to the CEO during the years of 2001 to 2003. He is now working as a research assistant in E. L. Ginzton Laboratory, Stanford University. His research interests include MEMS technology, micromachined ultrasonic devices, and medical devices. Mr. Lin was a recipient of the National Ministry of Education Award, Taiwan, in 2004.

Serena H. Wong was born in Stanford, CA. She received her B.S. and M.S. degrees in electrical engineering from Stanford University, Stanford, CA, in 2002 and 2003, respectively. She is currently a Ph.D. candidate in electrical engineering at the E. L. Ginzton Laboratory of Stanford University. She is a 2002 National Science Foundation Fellow, 2002 Stanford Graduate Fellow, and a member of Tau Beta Pi.

From 1998 through 2001, she worked as a research assistant in the Pre-polarized Magnetic Resonance Imaging (pMRI) laboratory at Stanford University in an effort to develop a cost-effective MRI system. This system would greatly reduce costs of imaging technology and improve accessibility for patients. Recently, she has been interested in high intensity focused ultrasound (HIFU) as a minimally-invasive therapeutic

tool for treatment of arrythmias and cancer. She is developing a non-invasive, MR-guided, therapeutic ultrasonic transducer for treatment of liver tumors.

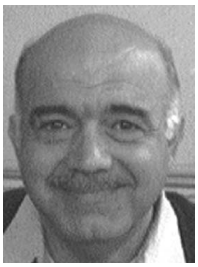

Butrus T. Khuri-Yakub (S'70–S'73–M'76–SM'87–F'95) was born in Beirut, Lebanon. He received the B.S. degree in 1970 from the American University of Beirut, the M.S. degree in 1972 from Dartmouth College, Hanover, NH, and the Ph.D. degree in 1975 from Stanford University, Stanford, CA, all in electrical engineering. He joined the research staff at the E. L. Ginzton Laboratory of Stanford University in 1976 as a Research Associate. He was promoted to a Senior Research Associate in 1978, and to a Professor of Electrical Engineering (Research) in 1982. He has served on many university committees in the School of Engineering and the Department of Electrical Engineering.

Presently, he is the Deputy Director of the E. L. Ginzton Laboratory, and the associate chairman for graduate admissions in the electrical engineering department at Stanford. Professor Khuri-Yakub has been teaching both at the graduate and undergraduate levels for more than 20 years, and his current research interests include *in situ* acoustic sensors (temperature, film thickness, resist cure, etc.) for monitoring and control of integrated circuits manufacturing processes, micromachining silicon to make acoustic materials and devices such as airborne and water immersion ultrasonic transducers and arrays, and fluid ejectors, and in the field of ultrasonic nondestructive evaluation and acoustic imaging and microscopy.

Professor Khuri-Yakub is a fellow of the IEEE, a senior member of the Acoustical Society of America, and a member of Tau Beta Pi. He is associate editor of *Research in Nondestructive Evaluation*, a Journal of the American Society for Nondestructive Testing. Professor Khuri-Yakub has authored more than 400 publications and has been principal inventor or co-inventor of 60 issued patents. He received the Stanford University School of Engineering Distinguished Advisor Award, June 1987 and the Medal of the City of Bordeaux for contributions to NDE, 1983.